NMR Characterization of Three-Disulfide Variants of Lysozyme, C64A/C80A, C76A/C94A, and C30A/C115A—A Marginally Stable State in Folded Proteins

Atsushi Yokota,[‡] Kenichi Hirai,[§] Hiroyo Miyauchi,[§] Satoshi Iimura,[§] Yasuo Noda,[§] Kyoko Inoue,[||] Kazuyuki Akasaka,[⊥] Hideki Tachibana,[#] and Shin-ichi Segawa*[,§]

Japan Science and Technology Corporation, Izumi, Osaka, 594-1144, Japan, Department of Physics, School of Science and Technology, Kwansei Gakuin University, Sanda, 669-1337, Japan, Genome Science Center, RIKEN Yokohama Institute, Yokohama, 230-0045, Japan, Kinki University, School of Biology-Oriented Science and Technology, Wakayama, 649-6493, Japan, and Department of Biology, Faculty of Science, and Graduate School of Science and Technology, Kobe University, Kobe, 657-8501, Japan

Received January 5, 2004; Revised Manuscript Received March 31, 2004

ABSTRACT: Our earlier NMR study showed that a two-disulfide variant of hen lysozyme containing intra-α-domain disulfide bridges, C6−C127 and C30−C115, is partially folded, with the α domain tightly folded to the nativelike conformation and the β domain flexible or unfolded. With a view that the formation of a third disulfide bridge is a key for the accomplishment of the overall chain fold, three-dimensional structures of three-disulfide variants of hen lysozyme lacking one disulfide bridge (C64A/C80A, C76A/C94A, and C30A/C115A) were studied in detail using NMR spectroscopy. Amide hydrogen exchange rates were measured to estimate the degree of conformational fluctuation in a residue-specific manner. The structure of C76A/C94A was found to be quite similar to that of the wild type, except for the peptide segment of residues 74−78. The structure of C64A/C80A was considerably disordered in the entire region of the loop (residues 62−79). Further, it was found that a network of hydrogen bonds within the β sheet and the 3_{10} helix in the β domain were disrupted and fluctuating. In C30A/C115A, the D helix was unstructured and the interface of the B helix with the D helix was significantly perturbed. However, the structural disorder generated in the hydrophobic core of the α domain was prevented by the C helix from propagating toward the β domain. A marginally stable state in folded proteins is discussed based on the structures remaining in each three-disulfide variant.

Wild-type hen lysozyme is composed of two domains: an α domain (residues 1−39 and 88−129) and a β domain (residues 40−87). There exists a hydrophobic core enclosed by four helices (from A to D) in the α domain. Wild-type lysozyme has four disulfide bridges: C6−C127, C30−C115, C64−C80, and C76−C94, of which C6−C127 combines the C terminus with the N terminus, C30−C115 is located in the hydrophobic core, C64−C80 in the β domain, and C76−C94 at the interface between the α and β domains (Figure 1). In general, the fully reduced protein attains native disulfide pairings through one-, two-, and three-disulfide intermediates, etc., during the oxidative refolding. To understand the pathway of folding well, knowledge on the structures and stability of the intermediates is crucial. Stable analogues of such intermediates can be prepared as variants lacking a specific disulfide bridge by amino acid substitution for the Cys residue. In the case of hen lysozyme, three-disulfide (3SS)[1] variants, C6S/C127A, C30A/C115A, C64A/C80A, and C76A/C94A, can mimic 3SS-intermediates lacking a corresponding disulfide bridge. The structures of these 3SS variants have been studied mainly by means of CD spectroscopy (*1*−*3*). All of the 3SS variants showed near-UV CD spectra characteristic of the native protein. To reveal structural differences between 3SS variants in detail, NMR structural analysis has become indispensable. So far, NMR structural studies of such disulfide regeneration intermediates in oxidative refolding have been carried out in some proteins: BPTI (*4*, *5*), RNase (*6*, *7*), and hen lysozyme (*8*).

In the case of lysozyme, two species of hen lysozyme derivatives lacking one disulfide bridge have been studied in detail by means of NMR spectroscopy or X-ray crystallography. One is the Cys6, Cys127-carboxymethylated derivative of lysozyme (6,127-rcm-lysozyme), which is the analogue of C6S/C127A (*9*, *10*), and the other is a kinetically trapped three-disulfide intermediate during oxidative refolding, des-[76−94], which is the analogue of C76A/C94A (*8*).

* To whom correspondence should be addressed. Phone: +81-79-565-8482. Fax: +81-79-565-9077. E-mail: shsegawa@kwansei.ac.jp.
‡ Japan Science and Technology Corporation.
§ Kwansei Gakuin University.
|| RIKEN Yokohama Institute.
⊥ Kinki University.
Kobe University.

[1] Abbreviations: metLYZ, recombinant hen lysozyme containing the extra N-terminal Met; 3SS, three disulfide; C64A/C80A, 3SS variant of hen lysozyme with Ala64 and Ala80 substituted for Cys; C76A/C94A, 3SS varinat of hen lysozyme with Ala76 and Ala94 substituted for Cys; C30A/C115A, 3SS varinat of hen lysozyme with Ala30 and Ala115 substituted for Cys; 2SS[6−127 and 30−115], hen lysozyme variant with Cys64, Cys76, Cys80, and Cys94 replaced by Ala and two disulfide bridges Cys6−Cys127 and Cys30−Cys115; CD, circular dichroism; DQF−COSY, double-quantum filtered correlation spectroscopy; HSQC, heteronuclear single-quantum coherence; NMR, nuclear magnetic resonance; NOE, nuclear Overhauser effect; NOESY, nuclear Overhauser effect spectroscopy; TOCSY, total correlation spectroscopy; 2D and 3D, two- and three-dimensional.

10.1021/bi049967w CCC: $27.50
Published on Web 05/07/2004

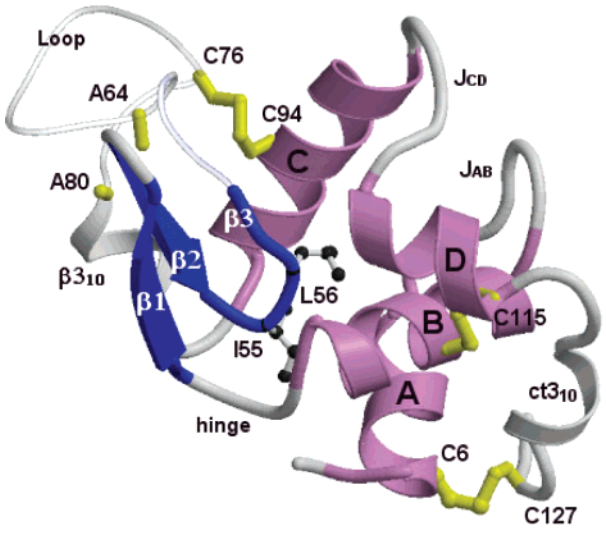

FIGURE 1: Ribbon diagram of a 3SS variant of hen lysozyme, C64A/C80A, produced by MolScript based on the X-ray crystallographic structure of the wild type (PDB 6LYZ). Four helices are colored magenta and construct the α domain of lysozyme: A (residues 4−15), B (residues 24−36), C (residues 89−99), and D (residues 108−115). The β sheet is colored blue: β1 (residues 41−46) and β2 (residues 50−54). The β3 strand drawn by a coil implicates that the segment is considerably perturbed. A thin tube shows the backbone from I58 to A80, where short- and long-range NOE contacts disappear. Yellow short sticks out of the backbone indicate the positions of A64 and A80 substituted for Cys. Sticks and balls represent the side chains of I55 and L56. J_{AB} and J_{CD} represent the joint region between the A and B helices (residues 16−23) and that between the C and D helices (residues 100−107), respectively. Two short 3_{10} helices are shown as $\beta 3_{10}$ (residues 80−84) and $ct3_{10}$ (residues 120−124).

The conformation of 6,127-rcm-lysozyme was extremely similar to that of the wild type, and differences were only slight except at the C terminus. On the other hand, NMR data for des-[76−94] showed that the differences in chemical-shift values from those of the wild type were somewhat large in the β domain and the interfacial region between the α and β domains, but des-[76−94] had a highly nativelike structure. The purpose of our paper is to characterize the structures of the other species of 3SS variants, C64A/C80A and C30A/C115A. Three species of 3SS variants, C64A/C80A, C76A/C94A, and C30A/C115A, were prepared, and the differences in structure and dynamic properties between them were studied in detail.

A detailed NMR structural study of the 2SS variant of lysozyme, 2SS[6−127 and 30−115] containing C6−C127 and C30−C115 in the α domain, revealed that the α domain of this variant is quite similar to that of the wild type, while the β domain is unstructured (*11*, *12*). In addition, experiments of oxidative refolding of lysozyme have shown that a complex ensemble of relatively unstructured intermediates with on average two disulfide bridges is rapidly formed, and then a kinetically trapped three-disulfide intermediate, des-[76−94], accumulates during oxidative refolding (*8*, *13*, *14*). Therefore, the structural differences between C64A/C80A and C76A/C94A are important to elucidate the role of the third disulfide bridge introduced to the 2SS variant. On the other hand, the disulfide bridge C30−C115 seems to have significant influence on the stability of the hydrophobic core in the α domain. The structure of C30A/C115A is important for characterizing a marginally stable state remaining in the α domain, because lysozyme variants lacking two disulfide bridges in the α domain have lost the overall structure.

EXPERIMENTAL PROCEDURES

Protein Expression and Purification. The method of production and purification of recombinant hen lysozyme, its 3SS variants, and uniformly ^{15}N-labeled samples has been described previously (*2*, *12*). Concentrations of the 3SS variants of lysozyme were estimated by using $A_{280} = 2.64$ for 1.0 mg/mL protein.

NMR Spectroscopy. The freeze-dried samples of the 3SS variants of lysozyme were dissolved in 95% H_2O/5% D_2O. The pH was adjusted to 3.8 by adding HCl or NaOH. 3D NMR spectra and 2D ^{1}H-^{1}H NMR spectra were measured at protein concentrations of about 1 mM. 2D ^{1}H-^{15}N HSQC spectra could be observed at lower protein concentrations (0.2 mM). Data were recorded at 600.13 MHz on a Bruker Avance 600 DRX spectrometer equipped with a Bruker/SGI workstation. ^{1}H-^{1}H DQF−COSY and NOESY (mixing time of 150 ms) experiments were carried out using standard procedures (*15*, *16*). Solvent signal suppression was achieved by using the WATERGATE scheme (*17*). Typically, data were collected at 1024 × 2048 data points in t_1 and t_2 directions with 64 transients. 2D ^{1}H-^{15}N HSQC spectra (*18*) were collected at 25 °C with 1024 × 2048 points in t_1 and t_2 directions, using uniformly ^{15}N-labeled samples. 3D NOESY−HSQC, TOCSY−HSQC (*19*), and HSQC−NOESY−HSQC (*20*) spectra were collected with 128 × 64 × 2048 in the t_1, t_2, and t_3 directions. Zero filling was applied prior to Fourier transformation, and data were processed with a shifted squared sine-bell window function in both dimensions.

Exchange of Amide Hydrogens. Amide hydrogens were exchanged in solution by dissolving the lyophilized protein in D_2O at pH 3.8. Acquisition of a ^{1}H-^{15}N HSQC spectrum was started within 20 min. Exchange reactions were followed with the change in the integrated volumes of ^{1}H-^{15}N cross-peaks of HSQC spectra, which were processed with FELIX 2000 (BioSym/MSI, San Diego, CA). The observed rates (k_{obs}) obtained by least-squares fitting were compared with the corresponding exchange rates (k_{int}) predicted according to Bai et al. (*21*) for completely unstructured hen lysozyme or its variants. As a result, protection factors (PFs) of each amide hydrogen were calculated as $PF = k_{int}/k_{obs}$.

RESULTS

NMR Spectra of 3SS Variants. ^{1}H-^{15}N HSQC spectra for C76A/C94A, C64A/C80A, and C30A/C115A were measured at pH 3.8 and 25 °C. All of them were basically similar to those of the recombinant hen lysozyme containing four intact disulfide bridges and an extra N-terminal Met (metLYZ) expressed in *Escherichia coli* (*12*). However, in the respective spectra, the positions of several cross-peaks moved greatly, and several ones disappeared or their peak intensities significantly weakened relative to those of metLYZ because of the removal of a specific disulfide bridge. Resonance assignments were carried out using 3D TOCSY−HSQC, 3D HSQC−NOESY−HSQC, and 3D NOESY−HSQC spectra. The procedures of the peak assignment are essentially the same as those described in our previous paper (*12*). In the HSQC spectra of C76A/C94A, C64A/C80A, and C30A/

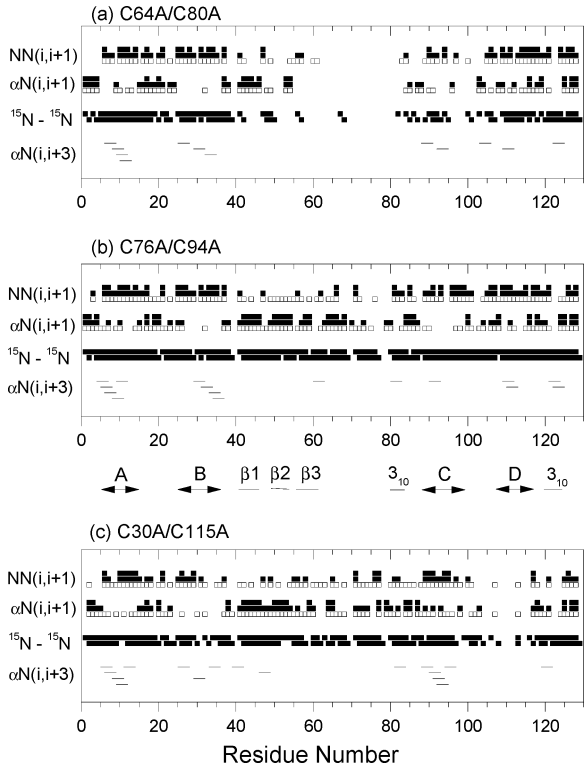

FIGURE 2: Summary of sequential and short-range NOE connectivities. NOE cross-peaks, NN(i, $i + 1$) and αN(i, $i + 1$), are classified into three groups according to their relative intensities; Open squares represent weak NOEs, and single- and double-filled squares denote medium and strong NOEs, respectively. ^{15}N-^{15}N represents sequential connectivities obtained from HSQC−NOESY−HSQC spectra. The upper and bottom symbols at the residue i correspond to the connectivity from i to $i + 1$ and that from $i - 1$ to i, respectively. The secondary structures observed in the wild-type lysozyme are indicated along the residue numbers. Continuous αN(i, $i + 3$) connectivities are indicative of the α-helical structure. (a) C64A/C80A, (b) C76A/C94A, and (c) C30A/C115A.

C115A, 125, 102, and 120 cross-peaks were identified for the backbone amide ^{1}H-^{15}N correlations, respectively.

NN(i, $i + 1$) and αN(i, $i + 1$) are NOE connectivities detected in the F1−F3 slice spectra of 3D NOESY−HSQC, where NN(i, $i + 1$) and αN(i, $i + 1$) denote ^{1}HN-^{1}HN and ^{1}Hα-^{1}HN cross-peaks between residues i and $i + 1$, respectively. In addition, F1−F3 slice spectra of HSQC−NOESY−HSQC give ^{15}N-^{15}N connectivities between neighboring residues. Figure 2 shows obtained NN(i, $i + 1$) and αN(i, $i + 1$) connectivities, where NOE cross-peaks are classified into weak, medium, and strong ones.

Strong NN(i, $i + 1$) and αN(i, $i + 1$) connectivities are usually indicative of an α helix and a β strand, respectively. In addition, short lines in Figure 2 represent observed αN(i, $i + 3$) connectivities, which are the strong indication that the polypeptide backbone adopts a regular helical structure. In C76A/C94A, strong NN(i, $i + 1$) and αN(i, $i + 1$) connectivities mean that the secondary structures of C76A/C94A are quite similar to those of the wild type. However, αN(i, $i + 3$) connectivities disappear within the C helix of C76A/C94A unlike the C helix of C30A/C115A. On the contrary, in C64A/C80A, strong NN(i, $i + 1$) are lost within the C helix and strong αN(i, $i + 1$) are also lost in the β2 and β3 strands, and further, almost all sequential NOE connectivities disappear in the region of residues 62−80. This indicates that the β domain of C64A/C80A is significantly perturbed. On the other hand, in C30A/C115A, NN(i, $i + 1$) are weakened within the B and D helices. In particular, ^{15}N-^{15}N connectivities are lost within the D helix, and αN(i, $i + 3$) are weakened within the B helix. However, strong αN(i, $i + 1$) detected in the entire region of the β sheet, strong NN(i, $i + 1$) found in the A and C helices, and especially αN(i, $i + 3$) within the C helix indicate that the structural disorder generated within the B and D helices does not propagate toward the C or A helix.

DQF−COSY spectra are available for resonance assignments of Hα, Hβ, and other side-chain protons, after backbone HN−Hα correlations have been identified. All of the chemical shift values identified at 25 °C are listed in the tables of the Supporting Information.

Map of Long-Range NOE Contacts. Long-range NOE contacts between residues i and j ($|i - j| \geq 5$) are important for the analysis of the three-dimensional structure of the protein. In general, they tend to be obtained between the side chain and the side-chain protons. In the 2D ^{1}H-^{1}H NOESY spectrum, many cross-peaks were well-separated from others in the spectral region below 1.0 ppm, between 5.2 and 7.0 ppm, or above 9.0 ppm along the F2 axis. As a result, 169, 117, and 150 long-range NOE contacts were obtained for C76A/C94A, C64A/C80A, and C30A/C115A, respectively. The map of long-range NOE contacts is shown against the residue number in Figure 3. Because multiple NOE contacts are found between the ith and jth residues, for example, HN(i)−Hβ(j), Hβ(i)−Hγ(j), etc., symbols indicating the NOE contact between a pair of residues vary in size and color according to the number of NOE contacts detected.

The contact map is divided into three regions: residues 1−39, 88−129 (α domain), and 40−87 (β domain). NOE contacts are grouped into some areas and labeled such as "B−D", "C−J_{AB}", "Cleft", etc. (see also Figure 1). The contact map of C76A/C94A is quite similar to that of metLYZ. The differences between them are limited only in the vicinity of residues 74−78. In C76A/C94A, many long-range NOE contacts still exist in "Loop" and "Cleft" regions. On the contrary, in the map of C64A/C80A, NOE contacts disappear entirely in the loop region (residues 62−79). Further, they are lost from the regions of "Cleft" and "$\beta 3_{10}-\beta$". Within the β sheet of C64A/C80A, NOE contacts between β1 and β2 strands just persist, but those between β2 and β3 strands are lost. However, it is interesting that I55 and L56 are properly embedded in the pocket surrounded by the A, B, and C helices, as indicated by "tn55-A", "tn55-B", and "tn55-C". In addition, NOE contacts found in the regions of "C−J_{AB}", "B−D", and "ct3_{10}−B", which are the interface between the N- and C-terminal halves of the α domain, give definitive evidence that the three-dimensional structure of the α domain of C64A/C80A is virtually the same as that of the wild type. The contact map of C30A/C115A is quite similar to that of metLYZ except for the region of "B−D". The interface between the B and D helices, which is a part of the hydrophobic core of the α domain, is significantly perturbed in C30A/C115A. On the other hand, many NOE contacts are definitely found in the region referred to as "C−J_{AB}", which is another part of the hydrophobic core. In the C-terminal region of this variant, NOE contacts with A and B helices are marginally secured.

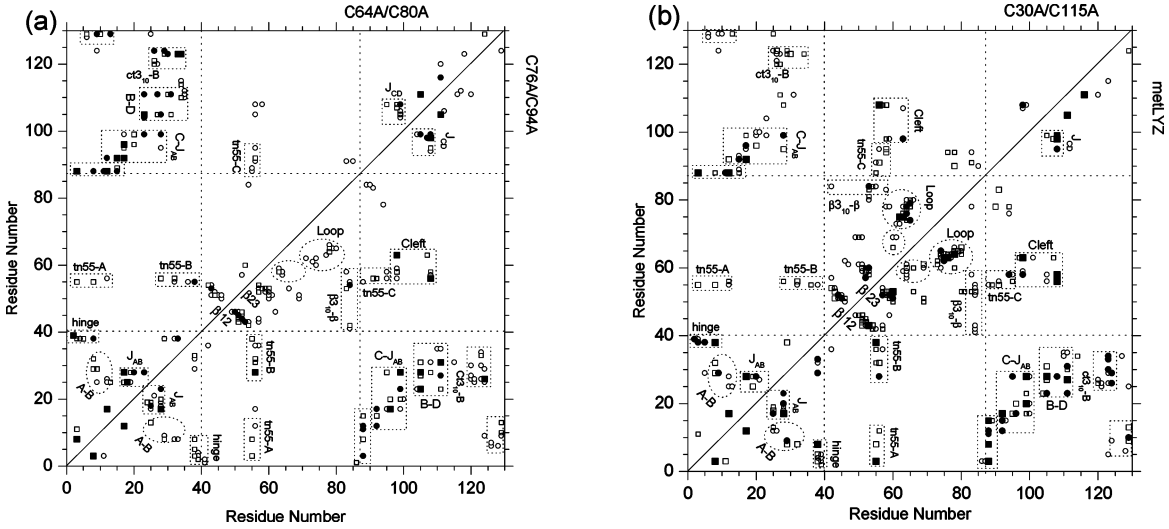

FIGURE 3: Long-range NOE contact map. (a) NOE contact maps of C64A/C80A (above the diagonal) and C76A/C94A (below the diagonal). (b) NOE contact maps of C30A/C115A (above the diagonal) and metLYZ (below the diagonal). In each map, symbols indicate long-range NOE contacts observed between protons of the *i*th residue and those of the *j*th residue, where $|i - j| \geq 5$. According to the number of NOE contacts detected between a specific pair of residues, the symbols vary in size and color. 1, (○); 2−3, (□); 4−5, (●); over 6, (■). Long-range NOE contacts are grouped and labeled (see text).

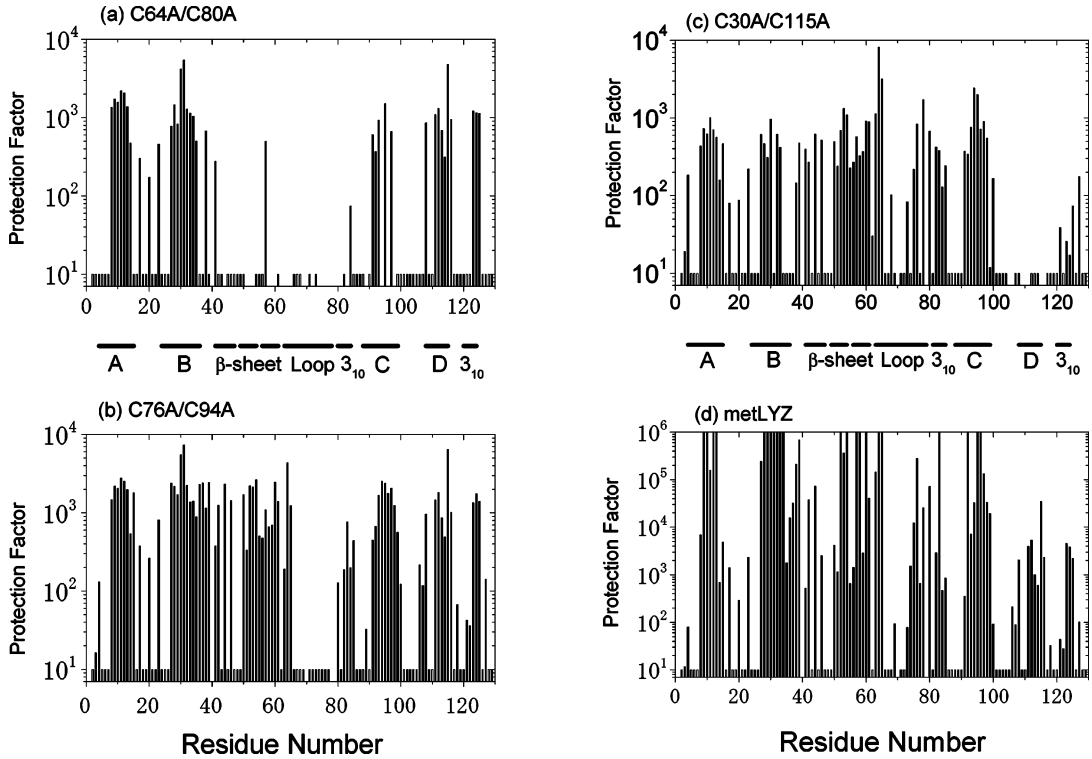

FIGURE 4: PFs of individual amide hydrogens against the HD exchange. (a) C64A/C80A, (b) C76A/C94A, (c) C30A/C115A, and (d) metLYZ. Short open columns represent amide hydrogens that are definitely detected in a H_2O solution but not in D_2O because of the fast exchange rate. Short bars along the abscissa indicate the secondary structures found in the wild-type lysozyme.

Structural Flexibilities of the 3SS Variants. To study the structural flexibility of the 3SS variants of lysozyme, amide hydrogen-exchange reactions were measured by following the time course of ^1H-^{15}N HSQC spectra. H−D exchange reactions were carried out at pH 3.8 and 25 °C for all protein samples. The PF of an individual amide hydrogen can be derived by comparing the exchange rate (k_{prot}) measured in a protein with the intrinsic rate (k_{int}) expected in a random coil model: $PF = k_{int}/k_{prot}$. The values of *PF* obtained are plotted against the residue number in Figure 4.

Hydrogen bonding of amide hydrogens and shielding them from the solvent generally protect the H−D exchange reaction. Proteins fluctuate around the time average structure and occasionally expose buried sites to the solvent. Thus, hydrogen-exchange reactions are mediated by local fluctuations in a protein structure (local unfolding) or the global unfolding of a protein. Amide hydrogens that are not exchangeable until the global unfolding occurs have the maximum *PF* of $1/K_{uf}$, where K_{uf} is the equilibrium constant of unfolding. Because the stability of the global structure of

the 3SS variants is greatly reduced by the loss of a single disulfide bridge, the maximum value of *PF* of the 3SS variants markedly decreases compared with that of metLYZ. The values of K_{uf} at 25 °C and pH 3.8 were estimated for respective proteins: 8.6×10^{-8} (metLYZ), 4.3×10^{-4} (C76A/C94A), 2.3×10^{-3} (C64A/C80A), and 2.7×10^{-3} (C30A/C115A).

In metLYZ, only the amide hydrogens involved in the center of the A, B, C helices and β sheet have PFs of more than 10^6 as shown in Figure 4d. Thus, exchange reactions of these amide hydrogens are mediated by the global unfolding, while amide hydrogens located at the peripheries of these secondary structures, 3_{10} helices and the D helix, are exchanged through structural fluctuations generated locally. In C76A/C94A, most amide hydrogens located in all of the helices, the β sheet, and the C-terminal 3_{10} helix are exchanged at similar rates nearly equal to $1/K_{uf}$ (about 2300). This means that PFs dominated by the global unfolding significantly decrease because of the removal of the disulfide bridge and become comparable to those ruled by the local unfolding, because the stability of local structures does not decrease so markedly as that of the global structure. Especially in the regions where PFs are less than 2000, they remain unaltered relative to those of metLYZ. Exceptionally, the PFs of residues 74−78 markedly decrease. These results suggest that the folded structure of C76A/C94A is as compact as that of the wild type except for the peptide segment around residue 76, despite the significant decrease in the stability of the global structure.

In C64A/C80A, besides the amide hydrogens rapidly exchanged in metLYZ, 45 amide hydrogens disappeared from the first HSQC spectrum after the initiation of the H−D exchange reaction. They are primarily the amide hydrogens of residues 42−85 and a part of residues 91−100. In the region of residues 58−83 of C64A/C80A, there are several residues whose cross-peaks are not identified in the HSQC spectrum measured in H_2O. However, the exchange rates of such amide hydrogens must be very fast, because all of the cross-peaks of C64A/C80A detected in D_2O are assigned to some residues already identified. The difference in the structural flexibility of the β sheet is marked between C64A/C80A and C76A/C94A. In C64A/C80A, the amide hydrogens of residues 42−64 and 80−85 are not protected at all, whereas they have definite PFs in C76A/C94A. On the other hand, A, B, and D helices and the C-terminal 3_{10} helix in the α domain of C64A/C80A have PFs dominated by the $1/K_{uf}$ (about 440). Thus, in C64A/C80A, the α domain is firmly protected against the H−D exchange as well as in C76A/C94A, while the entire region of the β domain fluctuates around the time average structure. Because the bridge C64−C80 combines the peptide segment 62−66 following the β3 strand with the 3_{10} helix (residues 80−84), its removal appears to perturb the spatial arrangement of the β3 strand and the 3_{10} helix. This may lead the overall structure of the β sheet to fluctuate largely.

In C30A/C115A, A and C helices, and the entire region of the β domain except for some residues have the PFs nearly equal to $1/K_{uf}$ (about 370). These regions seem to be tightly folded until the amide hydrogens are exposed to the solvent upon global unfolding. On the other hand, PFs in the C-terminal 3_{10} helix considerably decrease relative to those of other 3SS variants. In particular, amide hydrogens are no longer protected within the D helix and at the interface of the B helix (A31, F34, E35, S36, and N37) with the D helix.

DISCUSSION

Characterization of the Three-Dimensional Structures of C64A/C80A and C76A/C94A. The present paper has revealed that C64A/C80A and C76A/C94A are considerably different from each other in details of the folded structures. In C76A/C94A, both α and β domains are tightly folded into a compact structure, and the interface between them is relatively stable despite the loss of the interdomain disulfide bridge C76−C94. These results are consistent with the characterization by ^{1}H NMR of the des-[76−94] 3SS intermediate (*8*) and with the crystallographic study on a human lysozyme variant, C77A/C95A (*22*). On the other hand, in C64A/C80A, not only the loop, but also the cleft found in the wild type is unstructured. Further, it is likely that a network of hydrogen bonds of the β sheet and the 3_{10} helix in the β domain are disrupted and fluctuating.

However, it should be noted that the PFs of the α domain are unaltered in both 3SS variants. This probably means that the cooperativity between the α and β domains of lysozyme is not so strong compared to that between the N- and C-terminal halves of the α domain. The coupling between the two domains is mediated only through the β3 strand neighboring the C helix and the part of I55 and L56 surrounded by A, B, and C helices. In C64A/C80A, the interface between the C helix and the β3 strand is unstructured, but the C helix is stably built into the α domain as well as in C76A/C94A through complementary interactions between the C helix and the N-terminal half of the α domain. The C helix properly built into the α domain is crucial in folding the β domain, because it makes both ends of the β domain (T40 and D87) close to each other. In C64A/C80A, the structure of the β domain is largely flexible, but the overall chain fold appears to be kept nativelike. In fact, the polypeptide segment of residues 40−54 makes a kink point around G49 such that the β1 and β2 strands run antiparallel to each other (Figure 3a). The strong propensity to form an antiparallel β sheet may originate in the fact that this polypeptide segment contains four Thr residues (T40, T43, T47, and T51), because the branched β carbon of Thr favors the extended structure (*23*). Further, I55 and L56 are firmly anchored to the position in the α domain, where both ends of the β domain also come together. This position looks like a pivot of the β domain (Figure 1). The largely flexible structure of the β domain seems a marginally stable state remaining in the β domain, which is maintained by the C helix and the pivot (I55 and L56) properly built into the α domain. Once the C helix is unfolded and the pivot is detached from the α domain, the β domain may be completely unfolded.

Marginally Stable State in C30A/C115A. The present paper on C30A/C115A revealed that the D helix and the interface of the B helix with the D helix are unstructured or fluctuating largely. Because the C-terminal region is combined with the A helix through the disulfide bridge C6−C127, the structural disorder generated in the D helix is expected to propagate in the direction of the N terminus, but actually it is prevented by the existence of the C helix tightly folded. Because the C helix is further stabilized by long-range interactions with the joint region of the A and B helices, the stability of the

C helix is cooperative with the spatial arrangement between the A and B helices. The structure remaining in the α domain of C30A/C115A seems marginal in stability, because half of the hydrophobic core of the α domain is disrupted and the other half is secured. Once the spatial arrangement between the A and B helices is perturbed because of some causes, it may lead to the cooperative disruption of the marginally stable state. In fact, the 2SS variant lacking two disulfide bridges in the α domain is fully unfolded.

Relationship between the Dynamic Properties of the β Domain Structure and Folding Kinetics. The folding rate of C76A/C94A was significantly retarded relative to C64A/C80A (*2*). This was explained to be due to the high activation of Gibbs energy of C76A/C94A folding, because it seems necessary for the folding to bring the residue 76 to the vicinity of residue 94 and it is likely to cause a significant decrease in entropy of the transition state. On the contrary, C64A/C80A could fold into the compact structure as fast as the wild type. This meant that C64A/C80A folding might have occurred with leaving two segments around residues 64 and 80, not associated with each other, because of the presence of the bridge C76−C94, so that the activation energy of folding did not increase so much. In a similar way, the unfolding rate of C64A/C80A was much faster than that of C76A/C94A because the free-energy barrier against C64A/C80A unfolding was significantly lowered. These results and arguments are quite consistent with the static and dynamic properties of the folded structures of C64A/C80A and C76A/C94A, revealed in this paper.

On the other hand, a dominant oxidative folding intermediate of reduced denatured lysozyme was found to be the des-[76−94] 3SS species (*8*). This paper showed that the formation of the fully native protein was significantly accelerated by disulfide bridge rearrangements in the des-[76−94] 3SS species involving a substantial loss of structure. It was proposed that one interesting rearrangement process might involve the formation of the des-[64−80] 3SS species (*13*). These arguments are also consistent with the present paper on the folded structures of C64A/C80A and C76A/C94A.

Conversion from 2SS to 3SS Species. The removal of C76−C94 from the 3SS-variant C64A/C80A did not change the folded conformation significantly. In fact, the map of NOE contacts in 2SS[6−127 and 30−115] shown in the previous paper (*12*) is virtually the same as that of C64A/C80A, although the stability of the 2SS variant significantly decreases relative to the 3SS variant. These results are quite consistent with those caused by the removal of C76−C94 from the wild type. Thus, it is likely that the addition of C76−C94 to 2SS[6−127 and 30−115] does not contribute so much to the stabilization of the folded conformation itself but stabilizes the folded state relative to the unfolded one, primarily by accelerating the folding rate. On the other hand, the addition of C64−C80 to 2SS[6−127 and 30−115] appears to contribute mainly to the stabilization of the β domain and the deceleration of the unfolding rate.

ACKNOWLEDGMENT

This work was supported by a grant from the Ministry of Education, Culture, Sports, Science, and Technology, Japan (the High-Tech Research Center Project).

SUPPORTING INFORMATION AVAILABLE

Tables of ^{1}H chemical shift assignments of C64A/C80A, C76A/C94A, and C30A/C115A at 25 °C and pH 3.8. This material is available free of charge via the Internet at http://pubs.acs.org.

REFERENCES

1. Sawano, H., Koumoto, Y., Ohta, K., Sasaki, Y., Segawa, S., and Tachibana, H. (1992) Efficient in vitro folding of the three-disulfide derivatives of hen lysozyme in the presence of glycerol, *FEBS Lett. 303*, 11−14.
2. Yokota, A., Izutani, K., Takai, M., Kubo, Y., Noda, Y., Koumoto, Y., Tachibana, H., and Segawa, S. (2000) The transition state in the folding-unfolding reaction of four species of three-disulfide variant of hen lysozyme: the role of each disulfide bridge, *J. Mol. Biol. 295*, 1275−1288.
3. Tachibana, H., Ohta, K., Sawano, H., Koumoto, Y., and Segawa, S. (1994) Relationship between the optimal temperature of oxidative refolding and the thermal stability of refolded state of hen lysozyme three-disulfide derivatives, *Biochemistry 33*, 15008−15016.
4. van Mierlo, C. P. M., Darby, N. J., Neuhaus, D., and Creighton T. E. (1991) (14−38, 30−51) double-disulfide intermediate in folding of bovine pancreatic trypsin inhibitor: a two-dimensional ^{1}H nuclear magnetic resonance study, *J. Mol. Biol. 222*, 353−371.
5. van Mierlo, C. P. M., Darby, N. J., Keeler J., Neuhaus, D., and Creighton, T. E. (1993) Partially folded conformation of the (30−51) intermediate in the disulphide folding pathway of bovine pancreatic trypsin inhibitor, ^{1}H and ^{15}N resonance assignments and determination of backbone dynamics from ^{15}N relaxation measurements, *J. Mol. Biol. 229*, 1125−1146.
6. Laity, J. H., Lester, C. C., Shimotakahara, S., Zimmerman, D. E., Montelione, G. T., and Scherage, H. A. (1997) Structural characterization of an analog of the major rate-determining disulfide folding intermediate of bovine pancreatic ribonuclease A, *Biocheminstry 36*, 12683−12699.
7. Simotakahara, S., Rios, C. B., Laity, J. H., Zimmerman, D. E., Scheraga, H. A., and Montelione, G. T. (1997) NMR structural analysis of an analog of an intermediate formed in the rate-determining step of one pathway in the oxidative folding of bovine pancreatic ribonuclease A: automated analysis of ^{1}H, ^{13}C, and ^{15}N resonance assignments for wild-type and [C65S, C72S] mutant forms, *Biochemistry 36*, 6915−6929.
8. van den Berg, B., Chung, E. W., Robinson, C. V., and Dobson, C. M. (1999) Characterisation of the dominant oxidative folding intermediate of hen lysozyme, *J. Mol. Biol. 290*, 781−796.
9. Hill, C. P., Johnston, N. L., and Cohen, R. E. (1993) Crystal structure of a ubiquitin-dependent degradation substrate: A three-disulfide form of lysozyme, *Proc. Natl. Acad. Sci. U.S.A. 90*, 4136−4140.
10. Radford, S. E., Woolfson, D. N., Martin, S. R., Lowe, G., and Dobson, C. M. (1991) A three-disulfide derivative of hen lysozyme, *Biochem. J. 273*, 211−217.
11. Tachibana, H., Oka, T., and Akasaka, K. (2001) Native-like tertiary structure formation in the α-domain of a hen lysozyme two-disulfide variant, *J. Mol. Biol. 314*, 311−320.
12. Noda, Y., Yokota, A., Horii, D., Tominaga, T., Tanisaka, Y, Tachibana, H., and Segawa, S. (2002) NMR structural study of two-disulfide variant of hen lysozyme: 2SS[6−127, 30−15]−A disulfide intermediate with a partly unfolded structure, *Biochemistry 41*, 2130−2139.
13. van den Berg, B., Chung, E. W., Robinson, C. V., Mateo, P. L., and Dobson, C. M. (1999) The oxidative refolding of hen lysozyme and its catalysis by protein disulfide isomerase, *EMBO J. 18*, 4794−4803.
14. Roux, P., Ruoppolo, M., Chaffotte, A. F., and Goldberg, M. E. (1999) Comparison of the kinetics of S−S bond, secondary structure, and active site formation during refolding of reduced denatured hen egg white lysozyme, *Protein Sci. 8*, 2751−2760.
15. Cavanagh, J., Fairbrother, W. J., Palmer, A. G., III, and Skelton, N. J. (1996) *Protein NMR Spectroscopy: Principles and Practice*, Academic Press, San Diego, CA.
16. Bax, A. (1989) Two-dimensional NMR and protein structure, *Annu. Rev. Biochem. 58*, 223−256.

17. Piotto, M., Saudek, V., and Sklenar, U. (1992) Gradient-tailored excitation for single-quantum NMR spectroscopy of aqueous solutions, *J. Biomol. NMR 2*, 661−665.
18. Kay, L. E., Keifer, P., and Saarinen, T. (1992) Pure absorption gradient enhanced heteronuclear single quantum correlation spectroscopy with improved sensitivity, *J. Am. Chem. Soc. 114*, 10663−10665.
19. Marion, D., Driscoll, P. C., Kay, L. E., Wingfield, P. T., Bax, A., Gronenborn, A. M., and Clore, G. M. (1989) Overcoming the overlap problem in the assignment of ^{1}H NMR spectra of larger proteins by use of three-dimensional heteronuclear ^{1}H-^{15}N Hartmann−Hahn-multiple quantum coherence and nuclear Overhauser-multiple quantum coherence spectroscopy: application to interleukin 1 β, *Biochemistry 28*, 6150−6156.
20. Frenkiel, T., Bauer, C., Carr, M. D., Birdsall, B., and Feeney, J. (1990) HMQC−NOESY−HMQC, a three-dimensional NMR experiment which allows detection of nuclear overhauser effects between protons with overlapping signals, *J. Magn. Reson. 90*, 420−425.
21. Bai, Y., Milne, J. S., Mayne, L., and Englander, S. W. (1993) Primary structure effects on peptide group hydrogen exchange, *Proteins: Struct. Funct. Genet. 17*, 75−86.
22. Inaka, K., Taniyama, Y., Kikuchi, K., Morikawa, K., and Matsushima, M. (1991) The crystal structure of a mutant human lysozyme C77/95A with increased secretion efficiency in yeast, *J. Biol. Chem. 266*, 12599−12603.
23. Richardson, J. S., and Richardson, D. C. (1989) Principles and patterns of protein conformation, in *Prediction of Protein Structure and the Principles of Protein Conformation* (Fasman, G. D., Ed.) pp 1−98, Plenum, New York, NY.

BI049967W